Journal of Theoretical Biology 496 (2020) 110249

Contents lists available at ScienceDirect

Journal of Theoretical Biology

journal homepage: www.elsevier.com/locate/jtb

Change in telescoping leg strategy with varying walking speed to modulate force advantage

Seyoung Kim*, Cheolhoon Park, Chanhun Park

Department of Robotics and Mechatronics, Korea Institute of Machinery & Materials, 34103 156 Gajeongbuk-Ro Yuseong-Gu, Daejeon, Republic of Korea

ARTICLE INFO

Article history:
Received 30 July 2019
Revised 6 March 2020
Accepted 17 March 2020
Available online 19 March 2020

Keywords:
Human walking
Spring-like gait
Walking strategy
Telescoping leg
Force advantage

ABSTRACT

Human walking consists of two major sequential events (i.e., single- and double-support phases). Although there have been many studies relating to basic principles of the each stage, how the two distinct but continuous phases interact with each other remains to be clarified. We examined the change in walking strategy with varying walking speed on a local reference frame with telescoping and tangential axes; we expect that the telescoping directional dynamics at the end of a single-support phase change with walking speed to facilitate the modulation of the push-off work during a double-support phase. The telescoping directional force and power are calculated using two methods: model simulation and kinematic configuration. The empirical walking data for eight healthy young subjects and the corresponding model parameters obtained from a data-fit optimization were used to investigate the changing trend of each factor (i.e., force and power) with the increase in speed. The resulting force at the end of the single-support phase significantly increased with the walking speed for both methods, whereas the resulting power remained nearly unchanged and was close to zero for the entire range of walking speeds. This result implies that the positive amount of the telescoping directional force at the end of the single-support phase may be a certain type of preparation for the double-support phase, which can contribute to a larger push-off.

© 2020 Elsevier Ltd. All rights reserved.

1. Introduction

Several types of mechanical models, with a simplified framework of the center of mass (CoM) mechanics, have been employed to understand basic principles of human walking. Studies about the rigid inverted pendulum models with or without curved feet have described the dominance of the passiveness (Fathizadeh et al., 2019; Kumar et al., 2009; McGeer, 1993), stability of the limit cycle (Garcia et al., 1998; Pickle et al., 2018), and prediction of the collision impulse during step-to-step transition (Yeom and Park, 2010). In addition, they described the advantages of the rolling foot (Adamczyk et al., 2006), redirection of the CoM velocity (Adamczyk and Kuo, 2009), prediction of the preferred speed-step length relationship (Kuo, 2001), and major determinant of the metabolic cost (Donelan et al., 2002a). Furthermore, for the spring-like leg models, developed under the necessity of considering compliant properties of the leg, researchers have described the "M-shaped trajectory" of the vertical ground reaction force (GRF) (Blickhan et al., 2007; Geyer et al., 2006), small vertical oscillation of the body (Geyer et al., 2006), and reconstruction of the center of pressure (CoP) excursion (Whittington and Thelen, 2009).

In parallel with the investigations of the basic mechanisms of human walking, the following model-based approaches have been used to address the change in the walking strategy depending on the gait condition. 1) The modeling approach of incline walking suggests that the generation of optimal propulsion is gradually scaled with increasing incline slope to obey a biomechanical constraint (Oh et al., 2014). 2) The loaded walking approach that uses the spring-mass bipedal model shows that leg stiffness increases with the load such that the resonance-based oscillatory behavior of the CoM is maintained for a given walking speed (Lee et al., 2014). 3) Finally, the data-fit modeling approach using the energy-dissipative compliant leg demonstrates that the leg stiffness increases with speed to modulate the gait frequency and propulsion energy (Kim and Park, 2011).

Several studies have focused on a certain phase of walking to clarify its underlined mechanism or strategy. Mechanical energy balance between push-off and heel-strike is well maintained during the step-to-step transition, regardless of how it is defined (Adamczyk and Kuo, 2009), at four different walking speeds ranging from the preferred speed to the maximum speed (Kim and Park, 2012). Mechanics of single-support phase of walking was studied in depth by fitting a spring-loaded inverted pendulum

* Corresponding author.
E-mail addresses: seyoungkim@kimm.re.kr (S. Kim), parkch@kimm.re.kr (C. Park), chpark@kimm.re.kr (C. Park).

https://doi.org/10.1016/j.jtbi.2020.110249
0022-5193/© 2020 Elsevier Ltd. All rights reserved.

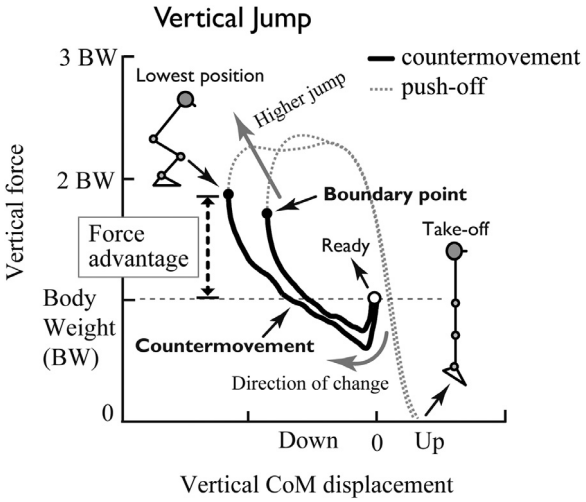

Fig. 1. Force–displacement (of the center of mass (CoM)) curves obtained from vertical jump experiments. Pilot tests were performed to reproduce the results presented in our previously published work (consistency confirmed). The black solid lines and dotted lines indicate the countermovement and push-off phases, respectively. The solid circles (i.e., boundary point) marked at the end of the countermovement indicate the lowest CoM position, whereas the hollow circle overlapped with body weight line indicates the starting position. The force advantage, which is the outcome of the countermovement, indicates the difference between the initial push-off force and subject's body weight. The gray-colored arrows represent the extension of the trajectories with increasing vertical jump height and the direction of change during the countermovement jump, respectively. Simple illustrations are included for a better understanding of the corresponding motion.

(SLIP) to empirical data: two contraction-expansion behavior (CECE cycle) during single-support phase plays an important role in energetically efficient walking (Antoniak et al., 2019). However, those studies did not consider the boundary between sequential phases of walking (e.g., single- and double-support phases) in terms of gait strategy.

Although not about walking, some recent studies have displayed interesting results about the standing vertical jump in which the boundary points on the force–displacement curve can be used to describe the strategy of the countermovement jump (Fig. 1) (Kim and Son, 2018; Kim et al., 2014). The boundary points are located between two sequential motion phases of countermovement and push-off, indicating that the points result from the countermovement action and serve as the initial advantage for the positive vertical acceleration and lowered CoM posture in the following push-off. More specifically, during the downward motion, the mechanical work performed by gravity and GRFs mainly contributes to the generation of downward momentum and resistive force against the momentum, respectively, resulting in the total work being cancelled out at the end of the countermovement phase. However, as part of the jumping strategy, the work-cancellation eventually produces a larger initial push-off force with increasing vertical jump height to facilitate the increase of the total push-off to create higher take-off velocities. This observation suggested that humans are aware of their body dynamics and select an appropriate movement strategy to meet the task goals (Kim and Park, 2011; Kim et al., 2014, 2009; Park et al., 2004).

Inspired by the concept of the countermovement strategy (i.e., boundary points), we assumed that if an appropriate reference frame is selected, meaningful outcomes could be determined between two major sequential phases of walking (i.e., single- and double-support phases) because the two phases have their own separate roles. The single-support phase plays a major role in the forward movement of the CoM, whereas the double-support phase, starting at the end of the single support phase, is responsible for redirecting the CoM velocity vector

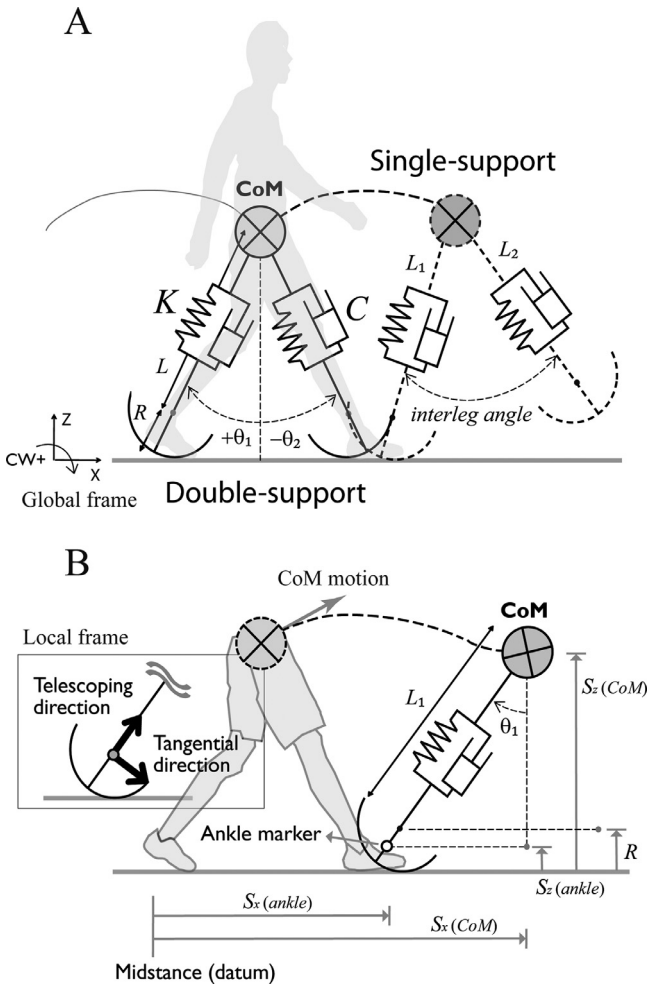

Fig. 2. (A) Schematic of the compliant walking model. The entire human body was modeled as a lumped mass with two massless, telescoping legs with curved feet. The parameters *K, C, θ, L,* and *R* indicate the spring constant, damping constant, leg angle with respect to the vertical axis, telescoping leg length, and radius (R = 0.3 m; fixed) of the curved foot, respectively. The subscripts "1" and "2" indicate the trailing and leading legs. A global horizontal–vertical reference frame is shown at the left bottom corner. (B) The model geometry for obtaining the leg angle (θ_1) and leg length (L_1) from the kinematic data. Parameters S_x and S_z indicate the horizontal distance from the midstance (datum), and the vertical distance from the ground; the parenthetical materials represent the corresponding objects, that is, the CoM or ankle marker. The leg angle (θ_1) is obtained using inverse tangent function with both the CoM and ankle marker positions (i.e., $\theta_1 = \tan^{-1}(\{S_x(CoM) - S_x(ankle)\}/\{S_z(CoM) - S_z(ankle)\})$, and the leg length ($L_1$) is then estimated using the pre-obtained leg angle, vertical CoM position, and curved foot radius as follows: $L_1 = \{S_z(CoM) - R\}/\cos\theta_1$. A local telescoping–tangential reference frame was located at the center of the curved foot (inset).

(Adamczyk and Kuo, 2009; Antoniak et al., 2019). We therefore thought that this approach can possibly describe the walking strategy.

In this study, we examined how walking strategy changes with speed on a local reference frame with telescoping and tangential axes that were defined based on the compliant walking model (Fig. 2): the aim of our study is to examine the question of "what happens in the telescoping direction". Primarily, the telescoping directional force and power, especially at the boundary between single- and double-support phases (i.e., at the end of the single-support phase), are calculated using two methods: model simulation and kinematic configuration. The empirical walking data for eight healthy young subjects obtained from ground-walking experiments with four speeds and the corresponding model parameters obtained from a data-fit optimization were used to investigate the

changing trend of each factor with increasing walking speed. Our integrative study utilizing models and experiments can contribute to the understanding of the human-walking strategy in terms of the telescoping directional force and power on a moving reference frame.

2. Methods

2.1. Subjects

Eight healthy young subjects (mean ± SD age, 23 ± 2 years; mean ± SD height, 168 ± 6 cm; mean ± SD body mass, 67 ± 11 kg), with no reported history of balance disorders or major leg injuries, participated in this study. After a detailed explanation of the purpose of the research and the possible use of collected data, all subjects signed an informed consent form approved by the Institutional Review Board of the KAIST.

2.2. Human walking experiments

The subjects walked on a straight walkway (12 m long × 1 m wide) at four speeds. Before the regular trials, their self-selected natural and maximum speeds were averaged from the initial setting procedure (i.e., ground-walking tests), and the corresponding frequencies were set as first and fourth gait frequencies, respectively. The second and third gait frequencies were then automatically determined between these two frequencies with the same intervals. Each subject conducted three sets of four randomly ordered walking experiments, in which the gait frequency cues were provided through a metronome (Dual Metronome Reference Pitch Generator SMT-1000, SAMICK, South Korea) with a steady beat, used as a steady-state walking guidance. With their preferred step length at each condition, actual walking speed for the subjects ranged from 0.8 to 2.2 m/s. The details of the experimental procedure have been presented previously (Kim and Park, 2011).

2.3. Measurements

Kinematic and kinetic data were measured using four motion-capture cameras (Hawk Digital Real-Time Camera, Motion Analysis, US) and three force plates (AccuGait, AMTI, US), respectively. Three optical markers were firmly attached on the sacrum (L5) and both ankles (lateral malleolus) of each subject. The sacral marker was used as an initial position to calculate the trajectory of the CoM, whereas the ankle markers were used to determine leg configurations. The reflective marker positions and GRFs were recorded at a sampling rate of 200 Hz and were filtered using a 5th-order Butterworth low-pass filter with cut-off frequencies of 10 and 30 Hz for the motion-capture and force-plate data, respectively. The cut-off frequencies that decoupled white noise from the raw data by minimizing the sum of residual error were determined through a residual analysis (Burkhart et al., 2011; Fekete et al., 2011; Salavati et al., 2009; Sinclair et al., 2013). Both the sacral marker position and GRF data were then used to estimate the velocity and position of the CoM by integrating the accelerations obtained from the GRF data, and the sacral marker was used to determine the integral constants (Donelan et al., 2002b; Kim and Park, 2011; Yeom and Park, 2010).

2.4. Compliant walking model

In this study, a human body was modeled as a lumped mass (CoM) with two massless, compliant legs with curved feet (Fig. 2A). A compliant leg is defined as a radial telescoping leg that deflects in the longitudinal direction with the use of an ideal spring–damper system but can transmit forces in the tangential directions, resulting in the CoM being on top of the compliant leg, which oscillates in the longitudinal direction, whereas the compliant leg rotates like a rigid inverted pendulum without bending in the tangential space.

A passive spring provided a telescoping mechanism to absorb collision impacts and generate push-off impulses, whereas a damper contributed to robust generation of repeated steps that reproduced the human data with various initial conditions. Both the spring and damper are assumed to be time-invariant linear components at a given walking speed. The curved foot is used to emulate CoP excursions throughout the gait cycle.

The dynamic equations of motion for the compliant walking model are derived through a *Newton–Euler* formulation, and then, the derived equations are compared with those from a *Lagrangian* formulation for confirmation. Consequently, the dynamic equations of the walking model can be written as follows (Eq. (1)) (Kim and Park, 2011; Whittington and Thelen, 2009):

$$\begin{bmatrix} MR\sin\theta_1 & M \\ ML_1^2 + 2MRL_1\cos\theta_1 + MR^2 & MR\sin\theta_1 \end{bmatrix} \begin{bmatrix} \ddot{\theta}_1 \\ \ddot{L}_1 \end{bmatrix} = \begin{bmatrix} ML_1\dot{\theta}_1^2 - Mg\cos\theta_1 + K(L_0 - L_1) - C\dot{L}_1 \\ +K(L_0 - L_2)\left(\dfrac{L_2\cos(\theta_1 - \theta_2) + R\cos\theta_1}{L_2 + R\cos\theta_2}\right) \\ -C\dot{L}_2\left(\dfrac{L_2\cos(\theta_1 - \theta_2) + R\cos\theta_1}{L_2 + R\cos\theta_2}\right) \\ -2ML_1\dot{L}_1\dot{\theta}_1 - 2MR\dot{L}_1\dot{\theta}_1\cos\theta_1 + MRL_1\dot{\theta}_1^2\sin\theta_1 + MgL_1\sin\theta_1 \\ +K(L_0 - L_2)\left(\dfrac{RL_2\sin\theta_2 - L_1L_2\sin(\theta_1 - \theta_2) - RL_1\sin\theta_1}{L_2 + R\cos\theta_2}\right) \\ -C_2\dot{L}_2\left(\dfrac{RL_2\sin\theta_2 - L_1L_2\sin(\theta_1 - \theta_2) - RL_1\sin\theta_1}{L_2 + R\cos\theta_2}\right) \end{bmatrix} \quad (1)$$

where M, g, R, θ, $\dot{\theta}$, $\ddot{\theta}$, L, $\dot{L}$, $\ddot{L}$, L_0, K, and C are the body mass, gravity constant, curved foot radius, leg angle, leg angular velocity, leg angular acceleration, leg length, leg length velocity, leg length acceleration, natural leg length (slack length), spring constant, and damping constant, respectively. The subscripts "1" and "2" indicate the trailing and leading legs, respectively.

2.5. Model parameters describing human walking with increasing speed

To simulate representative human walking, model parameters and initial conditions changing with walking speed were adopted from the previously published work because we have the same dynamic model consisting of exactly the same elements (Table 1) (Kim and Park, 2011). All the values listed in Table 1 were determined from empirical data, or at least based on it. Therefore, it is quite reasonable to use the values to overall describe the actual human walking.

The velocity and trajectory of the CoM were calculated by integrating the accelerations obtained from the GRF data (Donelan et al., 2002b; Kim and Park, 2011; Yeom and Park, 2010). Then, the natural leg length (slack length) of the model was estimated from the kinematic information (e.g., the CoM position, ankle marker position, and curved foot radius) at the end of the single support phase (Hong et al., 2013; Kim and Park, 2011). The curved foot radius was set to 0.3 m for all subject data based on previous literature showing that the fixed radius value could closely emulate center of pressure (CoP) excursions at slow, preferred, and fast walking speeds (Adamczyk et al., 2006; Whittington and Thelen, 2009).

With the basic parameters determined, spring and damping coefficients, which are key parameters of the compliant walking model, were originally estimated from an optimization that minimizes the fitting error between the experimental GRF data and

Table 1
Simulation parameters with increasing walking speed. Model parameters and initial conditions obtained from previous published studies* (Kim and Park, 2011) were given as a function of walking speed.

Human Walking Simulation with a simple Mass-Spring-Damper model				
	Parameter	*Value*	*Unit*	*Supporting details*
Condition	*Walking speed (W_{spd})*	0.8 ~ 2.2	*m/s*	• *Interval: 0.1 m/s*
Model parameters	*Body (CoM) mass*	66.7	*kg*	• *Average of all subjects*
	Body height	1.68	*m*	• *Average of all subjects*
	R (Curved foot radius)	0.3	*m*	• *Based on previous literatures**
	g (Gravity constant)	9.82	m/s^2	
	Interleg angle	$0.16 \cdot W_{spd} + 0.5$	*rad*	• *From prev. published work**
	C (Damping coefficient)	$120.24 \cdot W_{spd} - 71.15$	$N \cdot s/m$	• *From prev. published work**
	K (Spring coefficient)	$7.64 \cdot W_{spd} + 10.14$	*kN/m*	• *From prev. published work** • *Slightly tuned to maximize leg propulsion energy at the end of single-support phase*
Initial conditions	θ_1 *(Leg angle)*	$-0.08 \cdot W_{spd} - 0.18$	*rad*	• *From prev. published work**
	L_1 *(Leg length)*	$\underbrace{mean}_{N(W_{spd})=15}\ [(0.01 \cdot W_{spd} + 0.36)] \times bodyheight$	*m*	• *From prev. published work** • *Constant value because of the lack of significant difference*
	$\dot{\theta}_1$ *(Leg angular velocity)*	$(0.35 \cdot W_{spd} + 0.15) \times \sqrt{g/bodyheight}$	*rad/s*	• *From prev. published work**
	$\dot{L}_1$ *(Leg length velocity)*	$(-0.06 \cdot W_{spd} + 0.05) \times \sqrt{g \cdot bodyheight}$	*m/s*	• *From prev. published work**

model-driven trajectories. The estimated spring and damping coefficients were then employed to calculate the telescoping leg force (F_{leg}) produced by the trailing leg, with the simulated values of the leg length (L_1) and the leg length velocity ($\dot{L}_1$).

2.6. Model simulation and kinematic configuration

From the database (Table 1), the model parameters quantifying representative human walking as a function of gait speed are recruited to calculate the telescoping directional force, displacement, and power during the single-support phase (Fig. 3). The model parameters and initial conditions corresponding to each walking speed are input to simulate the single-support phase. The kinematic and kinetic trajectories are then estimated based on a local reference frame with telescoping and tangential axes (Fig. 2B; inset).

The amount of the total mechanical power on CoM (P_{CoM}) is divided into the telescoping component power (P_{tele}) and tangential component power (P_{tan}) for direction-based analysis (Eq. (2)), based on the local frame (Fig. 2B; inset).

$$\begin{aligned} P_{CoM} &= P_{tele} + P_{tan} \\ P_{tele} &= F_{tele} \cdot CoMvel_{tele} \\ P_{tan} &= F_{tan} \cdot CoMvel_{tan} \end{aligned} \tag{2}$$

where F_{tele}, F_{tan}, $CoMvel_{tele}$, and $CoMvel_{tan}$ are the telescoping directional force (i.e., sum of forces parallel to the telescoping axis), tangential directional force (i.e., sum of forces parallel to the tangential axis), CoM velocity in the telescoping direction, and CoM velocity in the tangential direction, respectively.

To understand the dynamics of CoM in the telescoping direction parallel to the line of action of the force produced by the trailing leg, we calculated the telescoping directional force (F_{tele}; resultant force) and power (P_{tele}; resultant power) as follows Eqs. (3) and ((4)):

$$\begin{aligned} F_{tele} = M \cdot \ddot{L}_{tele} = M \cdot \ddot{L}_1 = & \underbrace{\underbrace{K \cdot (L_0 - L_1) - C \cdot \dot{L}_1}_{spring\ damper} - \underbrace{M \cdot g \cdot \cos\theta_1}_{gravity}}_{F_{leg}} + \underbrace{\underbrace{M \cdot L_1 \cdot \dot{\theta}_1^2}_{L.frame\ rotation} - \underbrace{M \cdot R \cdot \ddot{\theta}_1 \cdot \sin\theta_1}_{L.frame\ translation}}_{F_{L.frame}} + \\ & \underbrace{\underbrace{K \cdot (L_0 - L_2)\left(\frac{L_2 \cdot cos(\theta_1 - \theta_2) + R \cdot cos\theta_1}{L_2 + R \cdot cos\theta_2}\right) - C \cdot \dot{L}_2\left(\frac{L_2 \cdot cos(\theta_1 - \theta_2) + R \cdot cos\theta_1}{L_2 + R \cdot cos\theta_2}\right)}_{load\ sharing\ during\ double-support\ phase}}_{F_{load.share}} \end{aligned} \tag{3}$$

$$\begin{aligned} P_{tele} = F_{tele} \cdot \dot{L}_{tele} &= \left(F_{leg} + F_{gravity} + F_{L.frame} + F_{load.share}\right) \cdot \dot{L}_1 \\ &= P_{leg} + P_{gravity} + P_{L.frame} + P_{load.share} \end{aligned} \tag{4}$$

where $\ddot{L}_{tele}(=\ddot{L}_1)$ is the trailing leg length acceleration in the telescoping direction. The telescoping directional force (F_{tele}) consists of four components (Eq. (3)): (1) force exerted by the trailing leg, described as a spring-damper system (F_{leg}), (2) force by gravity ($F_{gravity}$), (3) force exerted by the local frame's rotation and translation ($F_{L.frame}$), and (4) force due to load sharing between trailing and leading legs only during the double-support phase ($F_{load.share}$). As the local frame located at the center of the curved foot moves with the leg motion in space, the telescoping directional force (F_{tele}) has to be compensated according to the local frame rotation (*L. frame rotation* in Eq. (3)) and translation (*L. frame translation* in Eq. (3)) as much as necessary. Consequently, the telescoping directional power (P_{tele}) can also be split into four fragments: "power by trailing leg (P_{leg})", "power by gravity ($P_{gravity}$)", "power by local frame motion ($P_{L.frame}$)", and "power by load sharing ($P_{load.share}$)" (Eq. (4)).

Further, the kinematic configuration method is employed to confirm the trends in telescoping directional force and power Fig. 2B). The telescoping force and power during the single-support phase are calculated using geometrically obtained leg angle (θ_1) and leg length (L_1) from the kinematic data as follows (Eqs. (5) and (6):

$$\theta_1 = \tan^{-1}\left(\frac{S_x(CoM) - S_x(ankle)}{S_z(CoM) - S_z(ankle)}\right) \tag{5}$$

$$L_1 = \frac{S_z(CoM) - R}{\cos\theta_1} \tag{6}$$

The parameters S_x and S_z indicate the horizontal distance from midstance (datum) and the vertical distance from the ground, re-

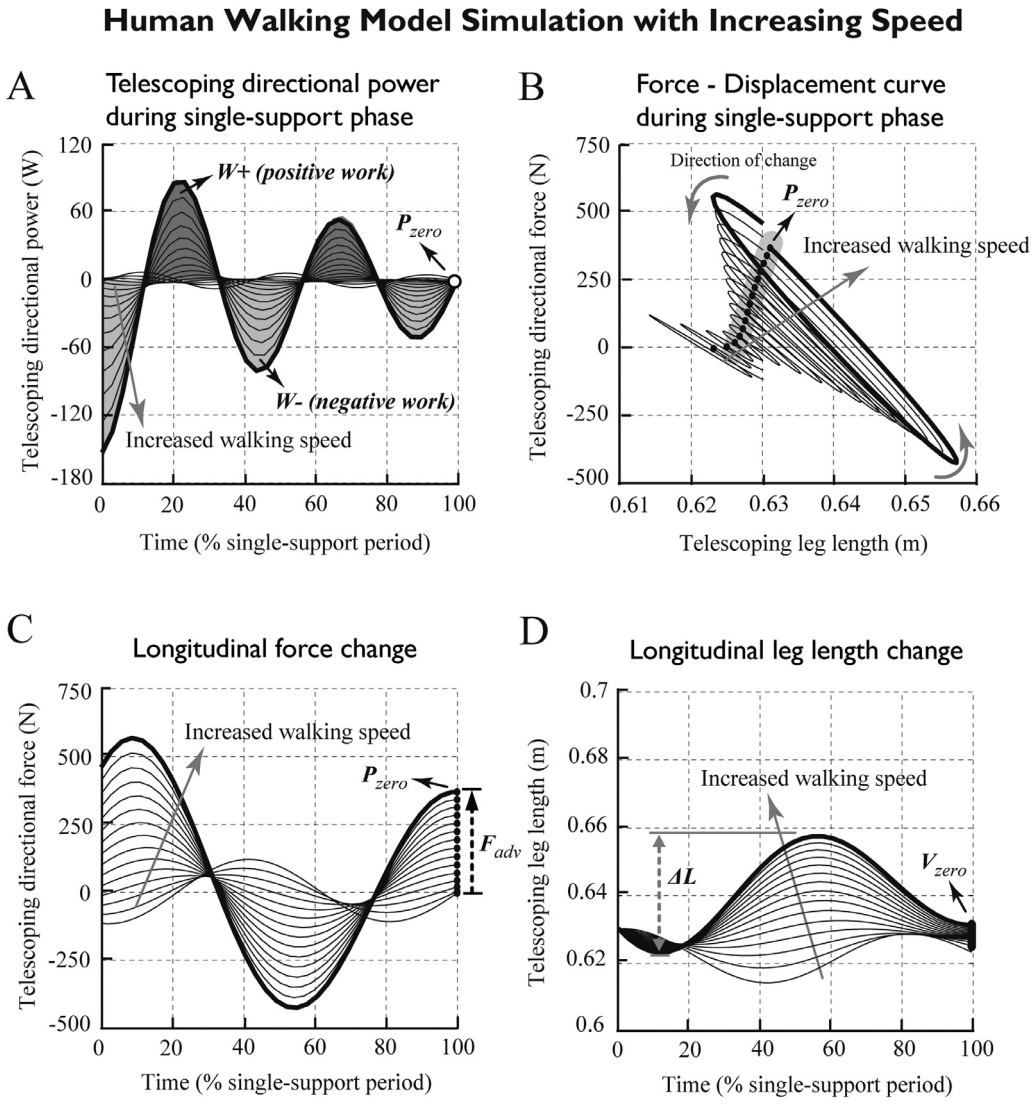

Fig. 3. Model simulation results with increasing walking speed. (A) Telescoping directional power (P_{tele}); (B) force–displacement curve; (C) telescoping directional force (F_{tele}); and (D) telescoping leg length ($L_{tele} = L_1$) during single-support phase. The time scales of the horizontal axis are presented as a percentage of the single-support period (A, C, and D). The shaded areas in (A) indicate the time-integrals of the corresponding power trajectory derived from the fastest walking speed, i.e., work performed on CoM (positive or negative: $W+$ or $W-$). V_{zero} is the zero-velocity point at the end of the single-support phase, where the power is zero (i.e., P_{zero}). The force advantage (F_{adv}) in (C) indicates the telescoping directional force (F_{tele}) at the end of the single-support phase; this is considered as the preparation for the following step, i.e., collision. The gray-colored arrows represent the extension of the trajectories with increasing walking speed and the direction of change during the single-support phase.

spectively, where the parenthetical materials represent the corresponding objects, that is, the CoM or ankle marker. The leg angle (θ_1) was obtained using the inverse tangent function of both the CoM and ankle marker positions (Eq. (5)), and the leg length ($L_1 = L_{tele}$) was then estimated using the pre-obtained leg angle, vertical CoM position, and curved foot radius (Eq. (6)). In addition, numerical differentiation of the obtained leg length (L_1) was also performed to estimate the telescoping directional force ($F_{tele} = M \cdot \ddot{L}_1$) and power ($P_{tele} = F_{tele} \cdot \dot{L}_1$).

As a result, the telescoping directional force (F_{tele}) and power (P_{tele}) at the end of the single-support phase were extracted from the single-support trajectories, and were sorted as a function of walking speed. The results were then plotted with the increasing walking speed and tested using linear regression model for both the model simulation (Fig. 4A and C) and kinematic configuration (Fig. 4B and D). To observe the mean trend of all subjects, we normalized the telescoping directional force data using the body weight (N) and the power data using the product of the body weight (N) and the square root of the leg length (m) multiplied by the gravitational acceleration (m/s^2). The significance of each of the reported trends from the parameter study was tested through regression analysis with a significance level of $P < 0.05$.

3. Results

3.1. Telescoping directional force, displacement, and power during single-support phase

The telescoping directional force-displacement curve in Fig. 3B shows a gradual scaling trend with walking speed. An elliptical trajectory shifts with increasing walking speed to yield both the larger peak force and leg length. For a faster walking speed, the force trajectory shows larger positive magnitudes in the beginning and ending points but smaller negative magnitude at the mid-stance compared with those of slower walking speed (Fig. 3C). This indicates that the force trajectories are crossed around the mid-stance on a time domain. In contrast, the telescoping leg shows a larger change in leg displacement (i.e., CoM displacement in

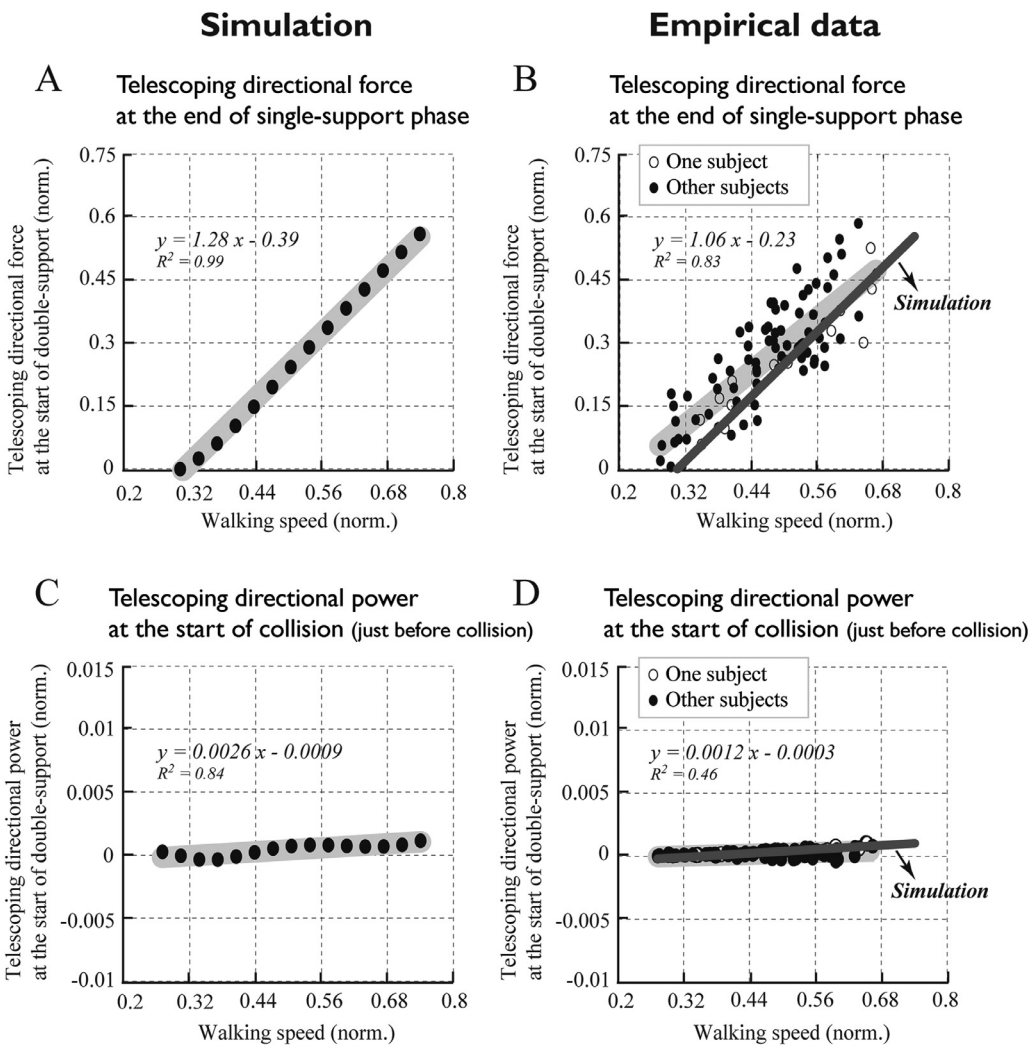

Fig. 4. Comparison of (A and C) model simulation and (B and D) kinematic configuration. (A and B) Telescoping directional force (F_{tele}) and (C and D) power (P_{tele}) at the end of the single-support phase. The hollow and solid black circles in B and D indicate one subject's data and other subjects' data respectively, where the thick dark gray lines indicate simulation results transferred from the graphs on the left side. The full equations for the curve fits (wide gray lines) are displayed in the form of $y = axe + b$, with the goodness-of-fit data. The normalization methods are described in the METHODS section.

the telescoping direction) around the midstance at a faster walking speed, as shown in Fig. 3D, in which the leg length trajectories seldom overlap on a time domain. Sequentially, calculating the dot product of the telescoping directional force (F_{tele}) and leg length velocity ($\dot{L}_1 = \dot{L}_{tele}$) produces sinusoidal power waveforms that cross the zero line during the single-support phase (Fig. 3A). The power trajectories start with negative magnitudes and end with nearly zero values during the single-support period, regardless of the walking speed, whereas the peak-to-peak values of the oscillations gradually decrease due to the damping effect.

3.2. Telescoping directional force and power at the end of the single-support phase

The telescoping directional force (F_{tele}) at the end of the single-support phase increased with walking speed ($P < 0.05$) (Figs. 4A and B), whereas the telescoping directional power (P_{tele}) remained nearly unchanged and was close to zero for the entire range of walking speeds (Fig. 4C and D). The increasing trend of the resulting force was clearly observed in both the model simulation (Fig. 4A) and the kinematic configuration method (Fig. 4B) with a certain level of goodness-of-fit data ($R^2 > 0.8$), whereas the resulting power showed no significant change from the zero value across the walking speeds (Fig. 4C and D). The changing trends obtained through the kinematic configuration are reasonably similar to those from the model simulation, as observed in the regression lines crossed with each other in a similar position (Fig. 4B and D). Additionally, the resulting forces at the end of the single-support phase were positive at all walking speeds (Figs. 3C; 4A and B), where all the endpoints have nearly zero CoM velocities in the telescoping direction (Fig. 3D), that is, near-zero powers at the end of the power trajectories (Figs. 3A; 4C and D).

3.3. Individual components of the telescoping directional force and power

The M-shaped telescoping leg force (F_{leg}) with positive values during the single-support phase mainly compensates for the gravity-driven force ($F_{gravity}$), resulting in the total sum of forces being parallel to the telescoping direction (F_{tele}), which has positive values in the beginning and ending parts of the single-support phase (Fig. 5A). In addition, the force generated by local frame motion ($F_{L.frame}$) shows positive but relatively small values compared with the values of the telescoping leg force (F_{leg}) and the gravity-driven force ($F_{gravity}$), whereas the force by load sharing

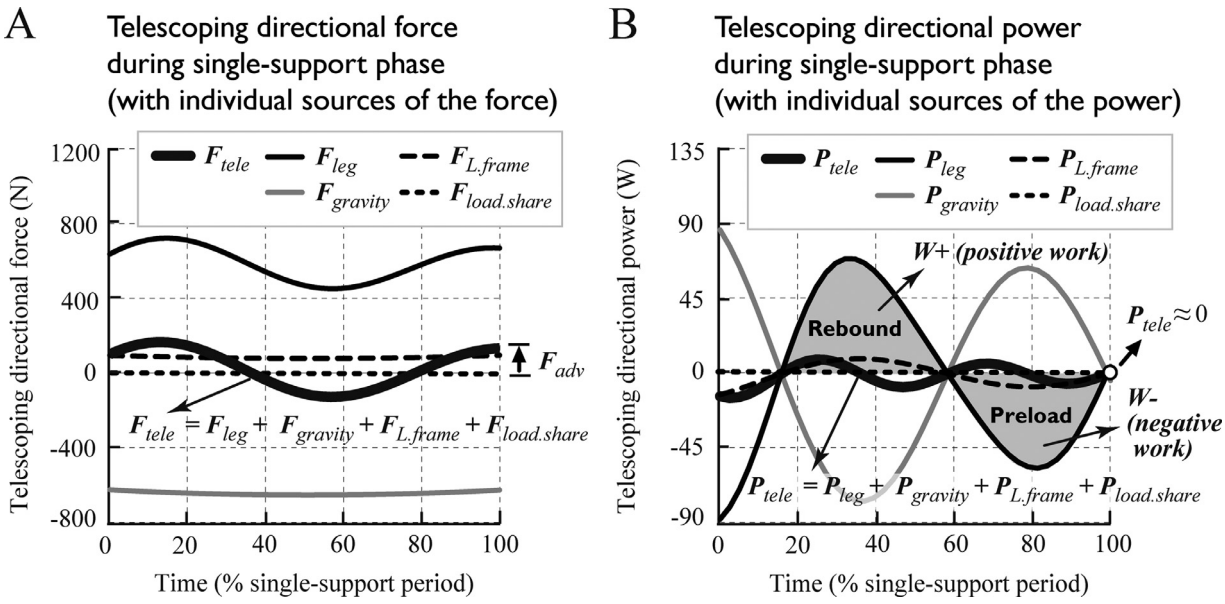

Fig. 5. Telescoping directional (A) force (F_{tele}) and (B) power (P_{tele}) during single-support phase at a walking speed of 1.4 m/s, shown with individual sources. The dark thick solid lines indicating F_{tele} and P_{tele} are the total sum of the corresponding four individual sources, where the sources come from "leg", "gravity", "Local frame motion", and "load sharing process during double-support phase". The shaded areas in (B) indicate the time-integrals of the corresponding power trajectory (P_{leg}) estimated from the spring-damper model (Fig. 2), i.e., work performed on CoM by the telescoping leg ($W+$: Rebound; $W-$: Preload).

($F_{load.share}$) has naturally zero value over the full single-support phase (Fig. 5A).

The power trajectories (P_{leg}, $P_{gravity}$, $P_{L.frame}$, and P_{tele}) showing several sign (+/-) changes depending on the sign of the leg length velocity ($\dot{L}_1$), finally converge close to zero because the leg length velocity ($\dot{L}_1$) ends with zero at the end of the single-support phase (Fig. 5B). Meanwhile, the external mechanical power by the trailing leg (P_{leg}) performed positive work (i.e., rebound) and negative work (i.e., preload) before and after midstance (Fig. 5B).

4. Discussion

4.1. Telescoping leg strategy modulates force advantage

Answer to "what happens in the telescoping direction": The positive amount of the telescoping directional force (F_{tele}) (i.e., the outcome; positive acceleration) at the end of single-support phase is a certain preparation for the double-support phase (Fig. 3C), which can contribute to a larger push-off (Fig. 6). Starting with the supportive initial force (i.e., F_{adv}; force advantage in Figs. 3C and 6) in the telescoping direction may facilitate in efficiently increasing the total push-off during the double-support phase in a limited time, when the telescoping directional CoM velocity at the start of the collision is nearly zero. The telescoping directional force (F_{tele}) starts progressively increasing at the beginning of double-support phase because of the emergence of the force produced by load sharing between the trailing and leading legs ($F_{load.share}$) (Fig. 6). Because the time-integrals of the telescoping directional force (F_{tele}) during the double-support phase (i.e., push-off impulse in the telescoping direction) play a key role in redirecting the CoM velocity vector (Adamczyk and Kuo, 2009; Park and Park, 2013), the initial force (F_{adv}) naturally helps to increase the total amount of the push-off impulse (i.e., work done on CoM). Simply put, "zero power (or velocity) but positive acceleration" would be the walking strategy during phase switching in the telescoping direction, occurring between the two sequential motion phases of walking, that is, the single- and double-support phases.

In addition, the telescoping leg strategy changes with walking speed to increase the amount of the initial telescoping directional force (F_{adv}) (Figs. 3C; 4A and B). Because of the CoM velocity redirection cost inevitably increasing with walking speed (Adamczyk and Kuo, 2009; Kim and Park, 2011; Park and Park, 2013), it is preferable to have a larger force preparation (i.e., force advantage in Fig. 3C) to reach the increased speed and maintain it at a certain level (i.e., steady-state walking). This supportive role of the telescoping leg strategy is directly related to the negative work performed by the trailing leg just before the collision (i.e., preload in Fig. 5B), where the negative work is only external mechanical work that humans actively produce. Due to the dynamics of a spring-loaded inverted pendulum, the corresponding power by the trailing leg (P_{leg}) has naturally the same sign with the power by the local frame motion ($P_{L.frame}$) during the preload, where the sum of the two powers mainly compensates for the gravity-driven power ($P_{gravity}$) (Fig. 5B). While the interplay among the individual sources (i.e., P_{leg}, $P_{gravity}$, $P_{L.frame}$) happens, the telescoping directional power (P_{tele}), i.e., the resultant power, shows one sign (+/-) change in the middle of the preload period, and finally converges to zero at the end of the single-support phase (Fig. 5B). Regardless of the walking speed, the telescoping directional power (P_{tele}) always converges close to zero (Fig. 3A), where the zero power point is identical to the point of maximum force advantage (F_{adv}) during the corresponding period (Figs. 3C and 5A), indicating that "zero power but positive acceleration depending on the walking speed" is one possible option for describing human-walking strategy.

Note that the suggested walking strategy could be determined because the relative coordinate with the telescoping and tangential axes (Fig. 2B) was appropriately selected to analyze the spring-like leg mechanics. If the strategy is based on the global reference frame (Fig. 2A), it would be difficult to observe "zero power but positive acceleration": complicating the definition or quantification of walking strategy.

This study may contribute to the understanding of the basic principles of the human-walking strategy in terms of the telescoping directional force and power on the moving reference frame. Furthermore, it would be interesting to extend this con-

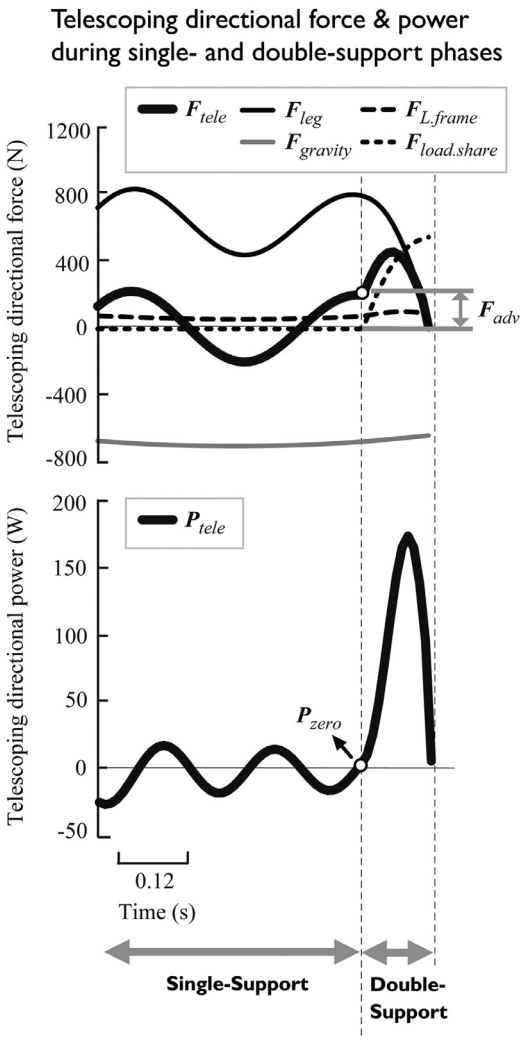

Fig. 6. Telescoping directional force (F_{tele}) (top) and power (P_{tele}) (bottom) during single- and double-support phases. The dark thick solid line indicates that F_{tele} (top) is the total sum of the corresponding four individual sources (e.g., F_{leg}, $F_{gravity}$, $F_{L.frame}$, and $F_{load.share}$). The hollow circles are located between two sequential motion phases of single- and double-support, where the power is nearly zero (i.e., P_{zero}).

cept to explore the relationship between "force advantage (F_{adv})" and "propulsion energy" with the approaches of previous studies suggesting that leg stiffness increases with speed to maximize the propulsion energy at the end of the single-support phase (Kim and Park, 2011). Additionally, it would be also very interesting to extend our scope to physiological interpretation of the spring-like leg mechanics. Because the walking model used in this study is basically a simple descriptive model for human center of mass dynamics, the spring-like leg behavior observed in the study needs to be interpreted considering both multi-joint and human physiological perspectives, to better understand real utilization of elasticity in human walking. For example, regarding the elastic elements in muscles, several studies have reported that Achilles tendon behaviors during single-support phase do not follow the spring-like bouncing concept, in which store and recoil of elastic energy occur in the first and second half of the single-support phase, respectively. Instead, the Achilles tendinous tissues were gradually stretched during the whole single-support phase and then recoiled during the double-support phase, whereas the corresponding muscle fascicles acted like a clutch to hold the spring-like Achilles tendon (Collins et al., 2015; Ishikawa et al., 2005; Sawicki and Khan, 2016).

4.2. CoM displacement in the telescoping direction increases with walking speed

The larger change in leg displacement (i.e., CoM displacement in the telescoping direction) around the midstance at a faster walking speed (Fig. 3D) is likely attributed to the selection of greater leg stiffness (K; increased up to 66%) with increasing tangential velocity ($L_1 \cdot \dot{\theta}_1$; increased up to 114%) (Table 1), where the leg stiffness and tangential velocity are directly related to the force pushing outward in the telescoping direction. From the physiological viewpoint, apart from joint kinematics analysis (not examined in this study), understanding the difference in the CoM displacement may require the assumption that soft tissue deformation is not negligible but obviously affects the sinusoidal CoM trajectory during human walking (i.e., Analysis of the CoM does not assume rigid bodies) (Fu et al., 2015; Zelik and Kuo, 2010). According to the previous literature (Zelik and Kuo, 2010), soft tissue elastic rebound occurring just before midstance could save up to 14% of the total positive work, although the contribution varied little with walking speed. Consequently, vertical displacement of the CoM during the single-support phase also increases with walking speed because of the increase of interleg angle (Fig. 2A; increased up to 37%) as well as the increase of the CoM displacement in the telescoping direction, which is consistent with previous literatures (Orendurff et al., 2004; Petrovic et al., 2019).

In addition, it is worth noting that the shorter single-support duration (i.e., smaller oscillation period of the walking model; decreased up to 32%) may be related to the increase in leg stiffness with increasing walking speed. Here, the single-support duration is generally allowable for one cycle of an oscillating motion, in view of physiologically plausible walking (Geyer et al., 2006; Kim and Park, 2011; Whittington and Thelen, 2009).

Declaration of Competing Interest

None.

CRediT authorship contribution statement

Seyoung Kim: Conceptualization, Methodology, Software, Formal analysis, Investigation, Writing - original draft, Writing - review & editing. **Cheolhoon Park:** Validation, Writing - review & editing. **Chanhun Park:** Validation, Writing - review & editing.

Acknowledgments

This research was supported by the R&D program of the Korea Institute of Machinery & Materials (KIMM), and the Alchemist project (No. 20007014) of Ministry of Trade, Industry and Energy (MOTIE).

References

Adamczyk, P.G., Kuo, A.D., 2009. Redirection of center-of-mass velocity during the step-to-step transition of human walking. J. Exp. Biol. 212, 2668–2678.
Adamczyk, P.G., Collins, S.H., Kuo, A.D., 2006. The advantages of a rolling foot in human walking. J. Exp. Biol. 209, 3953–3963.
Antoniak, G., Biswas, T., Cortes, N., Sikdar, S., Chun, C., Bhandawat, V., 2019. Spring-loaded inverted pendulum goes through two contraction-extension cycles during the single-support phase of walking. Biol. Open 8 bio043695.
Blickhan, R., Seyfarth, A., Geyer, H., Grimmer, S., Wagner, H., Günther, M., 2007. Intelligence by mechanics. philosophical transactions of the royal society a: mathematical. Phys. Eng. Sci. 365, 199–220. doi:10.1098/rsta.2006.1911.
Burkhart, T.A., Dunning, C.E., Andrews, D.M., 2011. Determining the optimal system-specific cut-off frequencies for filtering in-vitro upper extremity impact force and acceleration data by residual analysis. J. Biomech. 44, 2728–2731. doi:10.1016/j.jbiomech.2011.08.011.
Collins, S.H., Wiggin, M.B., Sawicki, G.S., 2015. Reducing the energy cost of human walking using an unpowered exoskeleton. Nature 522, 212–215. doi:10.1038/nature14288.

Donelan, J.M., Kram, R., Kuo, A.D., 2002a. Mechanical work for step-to-step transitions is a major determinant of the metabolic cost of human walking. J. Exp. Biol. 205, 3717–3727.

Donelan, J.M., Kram, R., Kuo, A.D., 2002b. Simultaneous positive and negative external mechanical work in human walking. J. Biomech. 35, 117–124.

Fathizadeh, M., Mohammadi, H., Taghvaei, S., 2019. A modified passive walking biped model with two feasible switching patterns of motion to resemble multi-pattern human walking. Chaos Solitons Fractals 127, 83–95. https://doi.org/10.1016/j.chaos.2019.06.018.

Fekete, T., Rubin, D., Carlson, J.M., Mujica-Parodi, L.R., 2011. The nirs analysis package: noise reduction and statistical inference. PLoS ONE 6, e24322. doi:10.1371/journal.pone.0024322.

Fu, X.-.Y., Zelik, K.E., Board, W.J., Browning, R.C., Kuo, A.D., 2015. Soft tissue deformations contribute to the mechanics of walking in obese adults. Med. Sci. Sports Exerc. 47, 1435–1443. doi:10.1249/MSS.0000000000000554.

Garcia, M., Chatterjee, A., Ruina, A., Coleman, M., 1998. The simplest walking model: stability, complexity, and scaling. J. Biomech. Eng. 120, 281–286.

Geyer, H., Seyfarth, A., Blickhan, R., 2006. Compliant leg behaviour explains basic dynamics of walking and running. Proc. R. Soc. B 273, 2861–2867.

Hong, H., Kim, S., Kim, C., Lee, S., Park, S., 2013. Spring-like gait mechanics observed during walking in both young and older adults. J. Biomech. 46, 77–82. doi:10.1016/j.jbiomech.2012.10.003.

Ishikawa, M., Komi, P.V., Grey, M.J., Lepola, V., Bruggemann, G.-.P., 2005. Muscle-tendon interaction and elastic energy usage in human walking. J. Appl. Physiol. 99, 603–608. doi:10.1152/japplphysiol.00189.2005.

Kim, S., Park, S., 2011. Leg stiffness increases with speed to modulate gait frequency and propulsion energy. J. Biomech. 44, 1253–1258. doi:10.1016/j.jbiomech.2011.02.072.

Kim, S., Park, S., 2012. The oscillatory behavior of the CoM facilitates mechanical energy balance between push-off and heel strike. J. Biomech. 45, 326–333. doi:10.1016/j.jbiomech.2011.10.009.

Kim, S., Son, Y., 2018. Mechanical work-canceling strategy modulates initial push-off force depending on vertical jump height. J. Mech. Sci. Technol. 32, 5345–5350. doi:10.1007/s12206-018-1033-8.

Kim, S., Park, S., Choi, S., 2014. Countermovement strategy changes with vertical jump height to accommodate feasible force constraints. J. Biomech. 47, 3162–3168. doi:10.1016/j.jbiomech.2014.06.013.

Kim, S., Horak, F.B., Carlson-Kuhta, P., Park, S., 2009. Postural feedback scaling deficits in Parkinson's disease. J. Neurophysiol. 102, 2910–2920.

Kumar, R.P., Yoon, J., Christiand, u., Kim, G., 2009. The simplest passive dynamic walking model with toed feet: a parametric study. Robotica 27, 701–713. doi:10.1017/S0263574708005079.

Kuo, A.D., 2001. A simple model of bipedal walking predicts the preferred speed-step length relationship. J. Biomech. Eng. 123, 264–269.

Lee, M., Kim, S., Park, S., 2014. Resonance-based oscillations could describe human gait mechanics under various loading conditions. J. Biomech. 47, 319–322. doi:10.1016/j.jbiomech.2013.09.011.

McGeer, T., 1993. Dynamics and control of bipedal locomotion. J. Theor. Biol. 163, 277–314.

Oh, K., Ryu, J.-.K., Park, S., 2014. A modeling study of mechanical energetic optimality in incline walking. J. Mech. Sci. Technol. 28, 1393–1401. doi:10.1007/s12206-014-0126-2.

Orendurff, M.S., Segal, A.D., Klute, G.K., Berge, J.S., Rohr, E.S., Kadel, N.J., 2004. The effect of walking speed on center of mass displacement. J. Rehabil. Res. Dev. 41, 829–834. doi:10.1682/jrrd.2003.10.0150.

Park, H.-.W., Park, S., 2013. Increase of push-off propulsion to compensate heel strike loss during step-to-step transition is limited at faster gait speeds. Int. J. Precis. Eng. Manuf. 14, 825–829. doi:10.1007/s12541-013-0108-9.

Park, S., Horak, F.B., Kuo, A.D., 2004. Postural feedback responses scale with biomechanical constraints in human standing. Exp. Brain. Res. 154, 417–427.

Petrovic, M., Maganaris, C.N., Bowling, F.L., Boulton, A.J.M., Reeves, N.D., 2019. Vertical displacement of the centre of mass during walking in people with diabetes and diabetic neuropathy does not explain their higher metabolic cost of walking. J. Biomech. 83, 85–90. doi:10.1016/j.jbiomech.2018.11.027.

Pickle, N.T., Wilken, J.M., Fey, N.P., Silverman, A.K., 2018. A comparison of stability metrics based on inverted pendulum models for assessment of ramp walking. PLoS ONE 13. doi:10.1371/journal.pone.0206875, e0206875–e0206875.

Salavati, M., Hadian, M.R., Mazaheri, M., Negahban, H., Ebrahimi, I., Talebian, S., Jafari, A.H., Sanjari, M.A., Sohani, S.M., Parnianpour, M., 2009. Test–retest reliabty of center of pressure measures of postural stability during quiet standing in a group with musculoskeletal disorders consisting of low back pain, anterior cruciate ligament injury and functional ankle instability. Gait Posture 29, 460–464. doi:10.1016/j.gaitpost.2008.11.016.

Sawicki, G.S., Khan, N.S., 2016. A simple model to estimate plantarflexor muscle-tendon mechanics and energetics during walking with elastic ankle exoskeletons. IEEE Trans. Biomed. Eng. 63, 914–923. doi:10.1109/TBME.2015.2491224.

Sinclair, J., Taylor, P.J., Hobbs, S.J., 2013. Digital filtering of three-dimensional lower extremity kinematics: an assessment. J. Hum. Kinet. 39, 25–36. doi:10.2478/hukin-2013-0065.

Whittington, B.R., Thelen, D.G., 2009. A simple mass-spring model with roller feet can induce the ground reactions observed in human walking. J. Biomech. Eng. 131, 011013. doi:10.1115/1.3005147.

Yeom, J., Park, S., 2010. A gravitational impulse model predicts collision impulse and mechanical work during a step-to-step transition. J. Biomech. 44, 59–67.

Zelik, K.E., Kuo, A.D., 2010. Human walking isn't all hard work: evidence of soft tissue contributions to energy dissipation and return. J. Exp. Biol. 213, 4257–4264. doi:10.1242/jeb.044297.